ACS Chemical Neuroscience
Cite This: ACS Chem. Neurosci. XXXX, XXX, XXX-XXX
Research Article
pubs.acs.org/chemneuro

In Vivo [^{18}F]GE-179 Brain Signal Does Not Show NMDA-Specific Modulation with Drug Challenges in Rodents and Nonhuman Primates

Matthias Schoenberger,[†,‡] Frederick A. Schroeder,[†] Michael S. Placzek,[†,§,#] Randall L. Carter,[∥] Bruce R. Rosen,[†,⊥] Jacob M. Hooker,[†,#] and Christin Y. Sander*[,†,#]

[†]Athinoula A. Martinos Center for Biomedical Imaging, Department of Radiology, Massachusetts General Hospital, Charlestown, Massachusetts 02129, United States

[‡]Chemical Biology and Imaging, Department of Pharmaceutical and Pharmacological Sciences, KU Leuven, BE-3000 Leuven, Belgium

[§]Department of Psychiatry, McLean Imaging Center, McLean Hospital, Belmont, Massachusetts 02478, United States

[∥]GE Global Research, Niskayuna, New York 12309, United States

[⊥]Harvard-MIT Division of Health Sciences and Technology, Massachusetts Institute of Technology, Cambridge, Massachusetts 02139, United States

[#]Harvard Medical School, Boston, Massachusetts 02115, United States

ABSTRACT: As one of the major excitatory ion channels in the brain, NMDA receptors have been a leading research target for neuroscientists, physicians, medicinal chemists, and pharmaceutical companies for decades. Molecular imaging of NMDA receptors by means of positron emission tomography (PET) with [^{18}F]GE-179 quickly progressed to clinical PET studies, but a thorough understanding of its binding specificity has been missing and has thus limited signal interpretation. Here a preclinical study with [^{18}F]GE-179 in rodents and nonhuman primates (NHPs) is presented in an attempt to characterize [^{18}F]GE-179 signal specificity. Rodent PET/CT was used to study drug occupancy and functional manipulation in rats by pretreating animals with NMDA targeted blocking/modulating drug doses followed by a single bolus of [^{18}F]GE-179. Binding competition with GE-179, MK801, PCP, and ketamine, allosteric inhibition by ifenprodil, and brain activation with methamphetamine did not alter the [^{18}F]GE-179 brain signal in rats. In addition, multimodal imaging with PET/MRI in NHPs was used to evaluate changes in radiotracer binding as a function of pharmacological challenges. Drug-induced hemodynamic changes were monitored simultaneously using functional MRI (fMRI). Comparisons of baseline and signal after drug challenge in NHPs demonstrated that the [^{18}F]GE-179 signal cannot be manipulated in a predictable fashion *in vivo*. fMRI data acquired simultaneously with PET data supported this finding and provided evidence that radiotracer delivery is not altered by blood flow changes. In conclusion, the [^{18}F]GE-179 brain signal is not readily interpretable in the context of NMDA receptor binding on the basis of the results shown in this study.

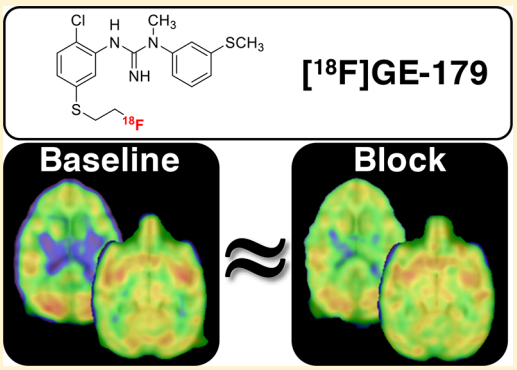

KEYWORDS: *NMDA receptors, [^{18}F]GE-179, PET/MRI, neuroreceptor imaging*

INTRODUCTION

NMDA receptors play a pivotal role in synaptic remodeling, learning, and memory formation.[1,2] They belong to the class of ionotropic glutamate receptors (iGluRs), which also includes AMPA and kainate receptors.[3] In contrast to other family members, NMDA receptors display noticeable conductivity for Ca^{2+} ions, enabling second messenger cascades that eventually change gene expression, triggering the structural changes that underlie synaptic remodeling.[4] To regulate these elements of signal transduction, NMDA receptor activation is guarded by multiple safety mechanisms that are unique among iGluRs: First, opening of the NMDA channel requires coagonism of both glycine and glutamate. It is worth recognizing that pentameric glycine receptors are chloride channels with an *inhibitory* effect and functionally counterbalance iGluRs, which are cation channels with an *excitatory* effect. Second, a Mg^{2+} ion blocks the NMDA channel pore and is expelled only when the membrane potential depolarizes, i.e., when the neuron is activated. In sum, three triggers—glycine agonism, glutamate agonism, and membrane depolarization—have to coincide in order for NMDA receptors to open.

Received: August 25, 2017
Accepted: October 19, 2017
Published: October 19, 2017

DOI: 10.1021/acschemneuro.7b00327
ACS Chem. Neurosci. XXXX, XXX, XXX−XXX

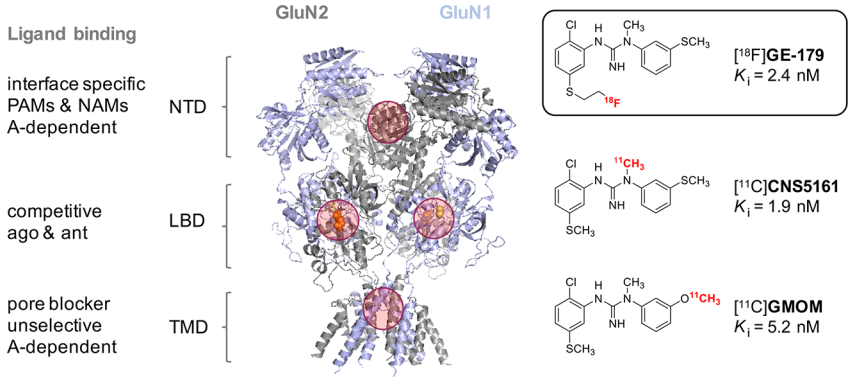

Figure 1. Structure of the NMDA protein crystal (PDB entry 4pe5).[5] NTD = N-terminal domain, LBD = ligand binding domain (referring to native ligands), TMD = transmembrane domain, PAM = positive allosteric modulator, NAM = negative allosteric modulator, A = activity, GluN2 = subunit that binds glutamate (shown as orange spheres), GluN1 = subunit that binds glycine (shown as yellow spheres). Four common drug binding sites are highlighted with red circles.

Structurally, NMDA receptors follow the classical design of a ligand-gated ion channel with an extracellular ligand binding domain (LBD) and an ion-conducting transmembrane domain (TMD).[6] Four distinct binding sites—described in Figure 1—are commonly addressed with small-molecule drugs:[7] (1) the phenylcyclidine (PCP) binding site, located in the channel pore in the TMD; (2) the clamshell domain of GluNR2, which binds the native agonist glutamate in the LBD; (3) the clamshell domain of GluNR1, which binds the native ligand glycine in the LBD; and (4) the interface of the dimer of dimers, located in the N-terminal domain (NTD). Positron emission tomography (PET) ligands have been developed as radiotracer candidates for all four binding sites (as reviewed by Fuchigami et al.[8]).

Ligands interacting with the pore region act by channel blocking, while agonists and antagonists of the clamshell domains act as competitive binders to the native agonists and ligands engaging the interface of the NTDs act by (negative or positive) allosteric modulation. Generally, channel blockers do not discriminate between NMDA receptor isoforms because of their high sequence homology in the pore region, but competitive or allosteric ligands often display selectivity for NMDA receptor subtypes.[9,10] Patch-clamp electrophysiology experiments revealed activity-dependent channel blockade by PCP-binding-site ligands, demonstrating that the channel has to be activated before the small molecule can act.[11] Furthermore, the term "trapped channel blocker" has been coined on the basis of patch-clamp studies that showed persistent blockade of activated channels long after washout of extracellular ligand.[12,13] Detailed understanding of these ligand−receptor interactions is pivotal for interpreting imaging data with the NMDA pore blocker [^{18}F]GE-179.

[^{18}F]GE-179 is an ^{18}F-labeled PET ligand from the class of bis(aryl)guanidine NMDA receptor blockers.[14,15] It is structurally related to the ^{11}C-labeled PET ligands CNS5161[16] and GMOM[17] (Figure 1) as well as the single-photon-emission computed tomography (SPECT) ligand [$^{123/125}$I]CNS1261.[19] *In vivo* molecular imaging of NMDA receptors by means of PET or SPECT has been attempted numerous times, and many ligands have progressed to human imaging.[8,20] However, to date no *in vivo* imaging probe has been established in routine research or clinical *in vivo* imaging applications because of the lack of specific, predictable binding to NMDA receptors.

In vivo imaging studies in healthy human subjects have shown that [^{18}F]GE-179 passes the blood−brain barrier (BBB) and displays tissue uptake in the striatum, thalamus, and cortex.[21] While the latter is consistent with NMDA receptor distribution, human [^{18}F]GE-179 signals also show relatively high uptake in the cerebellum, which has a low concentration of the target. In addition, evaluation of compartmental models in healthy human volunteers yielded good fits to a two-tissue compartment model with reversible binding. It is important to note that a trapped open-channel binding mechanism would lead to irreversible binding kinetics with no noticeable k_{off}. The possibility of anesthesia interfering with NMDA receptor states and associated probes has also been raised in previous investigations.[17,18] A dependence of [^{18}F]GE-179 on blood flow has also been suggested through a correlation between blood flow (K_1) and distribution volume (V_T).[21]

To date, there have been no published studies that directly demonstrate *in vivo* specificity of [^{18}F]GE-179 to NMDA receptors through drug competition studies or otherwise. Clinical research studies with [^{18}F]GE-179 are ongoing, and [^{18}F]GE-179 has been used to study patients with focal epilepsy.[22] Even though [^{18}F]GE-179 imaging showed a global increase in V_T compared with healthy controls, it remained unclear whether the signal corresponds to (activated) NMDA receptors.

Intrigued by the discrepancy between the established cellular blocking mechanism and the human *in vivo* binding kinetics and in order to determine whether [^{18}F]GE-179 imaging allows quantification of (activated) NMDA receptors *in vivo*, we performed a preclinical evaluation in rodents and nonhuman primates (NHPs) with PET/CT and PET/functional magnetic resonance imaging (fMRI).

RESULTS AND DISCUSSION

The preclinical experiments in rodents for evaluating the [^{18}F]GE-179 brain signal were designed to evaluate the effect of (i) occupying the PCP binding site with GE-179, MK801, PCP, or ketamine, (ii) allosteric inhibition at the NTD binding site with ifenprodil to prevent channel opening, and (iii) secondary/orthogonal modulation of NMDA activity through central nervous system (CNS) stimulants by methamphetamine. Male Sprague−Dawley rats were pretreated with the respective drug prior to receiving a bolus injection of [^{18}F]GE-179. A subset of the pharmacological challenges (unlabeled GE-179 and a CNS stimulant) were tested in NHPs using a within-scan challenge during bolus-plus-infusion of the radiotracer. The simultaneous acquisition of PET and fMRI in the NHP

DOI: 10.1021/acschemneuro.7b00327
ACS Chem. Neurosci. XXXX, XXX, XXX−XXX

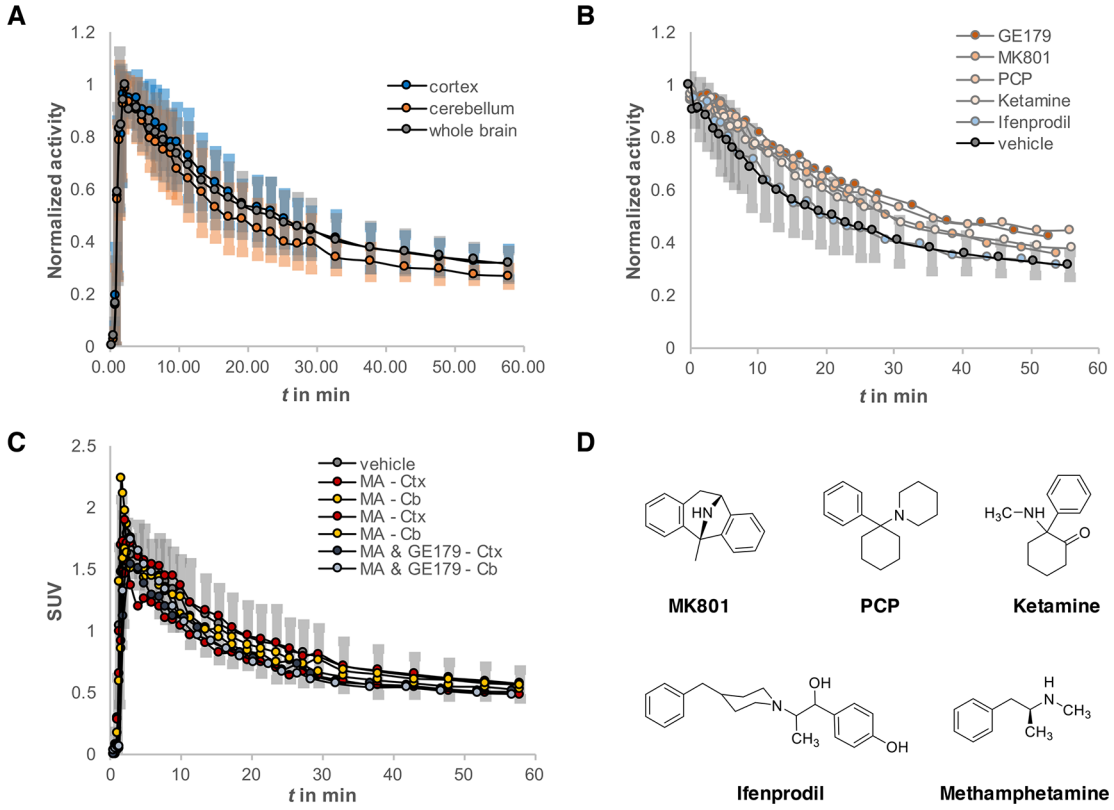

Figure 2. *In vivo* micro-PET imaging of [^{18}F]GE-179 in rats. (A) Time−activity curves (TACs) from vehicle-treated rats comparing whole brain (gray), cerebellum (orange), and cortex (blue), n = 3. Activity is normalized to peak uptake; error bars represent one standard deviation in each deflection. (B) Normalized whole-brain TACs comparing vehicle-treated rats (n = 3) and animals treated with MK801 (n = 1), PCP (n = 1), ketamine (n = 1), or ifenprodil (n = 1). (C) TACs showing the dynamic standard uptake value (SUV) of vehicle-treated rats (whole brain, gray, n = 3) as well as the cortex (Ctx) and cerebellum (Cb) of animals who received methamphetamine (MA) (n = 2) or a mixture of MA and GE-179 (n = 1). (D) Chemical structures of the drugs used to manipulate the *in vivo* [^{18}F]GE-179 signal.

enabled the assessment of probe-specific binding changes using PET while observing changes in neuronal activation patterns and hemodynamic changes resulting from the drug challenges.

***In Vivo* Rat Imaging and Drug Competition Experiments.** As a starting point for dissecting the nature of the *in vivo* [^{18}F]GE-179 signal, we pretreated rodents using the nonradioactive reference compound GE-179 as well as the commonly used NMDA channel blockers MK801, PCP, and ketamine,[23] which compete for the same binding site (Figure 2D). Animals were injected with either an equivalent volume of vehicle or a 1 mg/kg dose of the respective competition ligand 2 min prior to [^{18}F]GE-179 injection. Animals underwent a 60 min dynamic PET scan, and the subsequent time−activity curves (TACs) were evaluated to compare the slopes over the entire time course. Figure 2A displays TACs of the whole brain as well as the cortex (Ctx) and cerebellum (Cb) of three vehicle-treated rats, which served as a baseline for referencing drug challenges. There was no significant difference in slope between the whole-brain, Ctx, and Cb signals. To compare the effect of competitive drug challenges on [^{18}F]GE-179 binding, we normalized the standard uptake values (SUVs) to the initial peak uptake, hypothesizing that binding-site saturation would accelerate the washoff and reveal the extent of specific binding (Figure 2B). Interestingly, neither of the experiments led to a meaningful change in the whole-brain TAC, indicating that none of the *in vivo* [^{18}F]GE-179 signal at baseline represents displaceable binding. It could be hypothesized that the binding mode of a trapped channel blocker and a tightly controlled NMDA receptor homeostasis does not allow classical preoccupation or competition experiments. However, the whole-brain binding kinetics displays a clear dissociation and washout, which would invalidate the assumption that the signal represents a ligand−receptor interaction via a trapped binding mode.

Allosteric Inhibition. Further investigating the hypothesis that [^{18}F]GE-179 binds only open NMDA receptor channels, we employed the well-investigated negative allosteric modulator ifenprodil, which binds at the interface of the NR1 and NR2 subunits and stabilizes a closed channel conformation. Thus, no binding sites should be available for [^{18}F]GE-179, and its signal should represent nonspecific binding. However, the whole-brain TACs of ifenprodil-treated rats did not differ from those of vehicle-treated animals (Figure 2B), suggesting that the *in vivo* signal of [^{18}F]GE-179 in anesthetized rats does not represent activated NMDA receptors but rather nonspecific binding.

Orthogonal Activation. A possible explanation of this finding could be that even under baseline conditions, the effect of isoflurane anesthesia lowers the amount of glutamatergic activity to a minimum, yielding a very small population of open NMDA receptors. In this case, the available target density B_{max} would be too small to provide a meaningful signal-to-noise ratio even with a low-nanomolar binder such as [^{18}F]GE-179. To test this further, we used methamphetamine (MA) injections to trigger CNS activity (Figure 2C). MA is one of the strongest brain stimulants that targets the dopaminergic system and

DOI: 10.1021/acschemneuro.7b00327
ACS Chem. Neurosci. XXXX, XXX, XXX−XXX

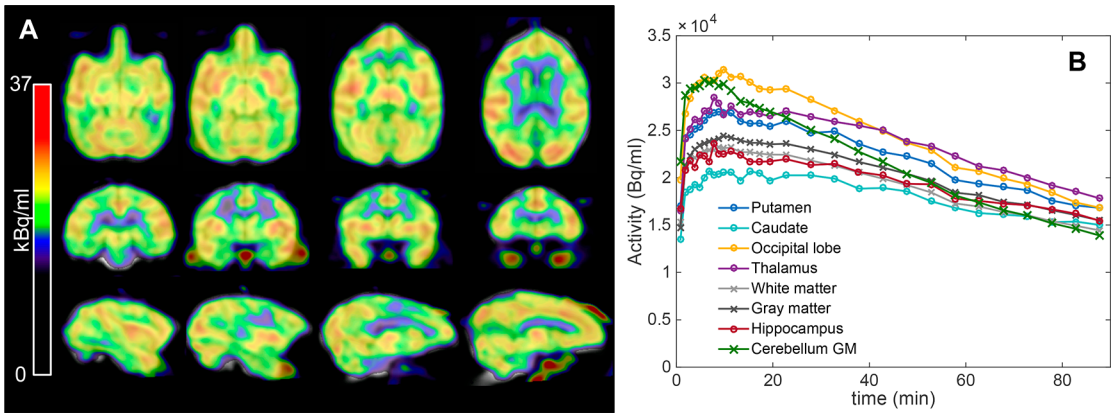

Figure 3. (A) Distribution of the [^{18}F]GE-179 baseline signal in a nonhuman primate. Voxelwise maps display the average signal over 20−50 min after tracer injection. (B) TACs for a variety of anatomical regions show reversible binding and dynamics similar to human data.

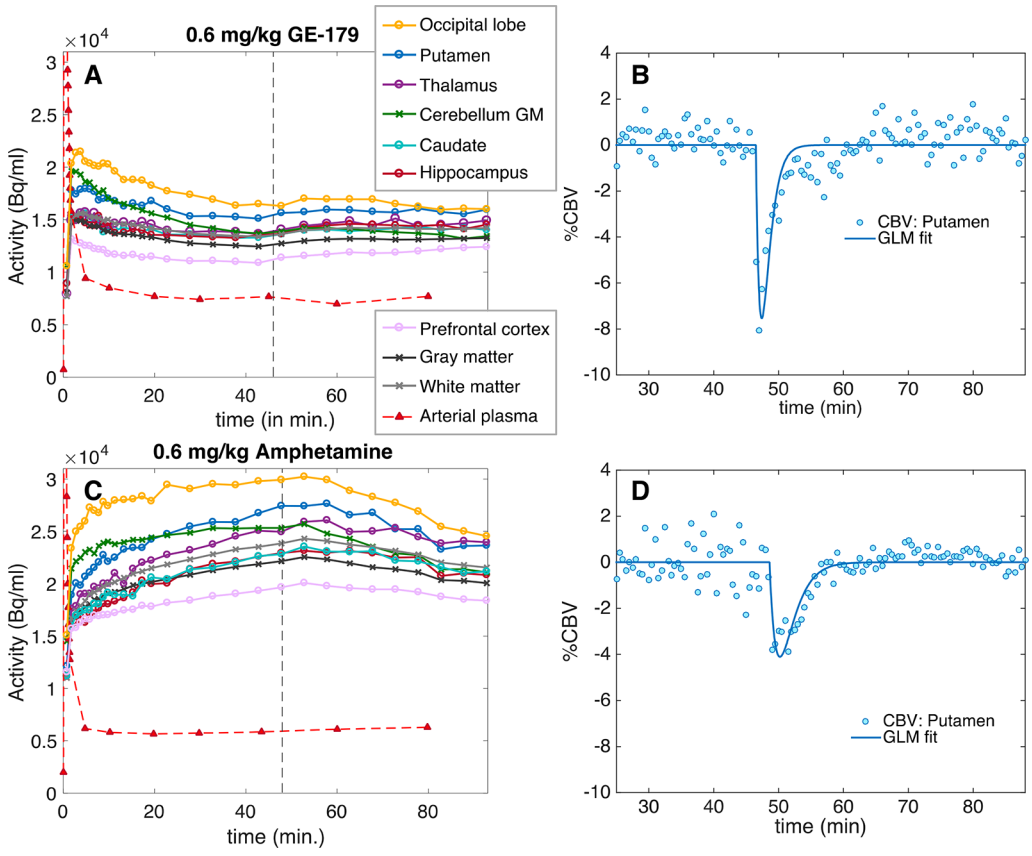

Figure 4. Simultaneously acquired PET and fMRI time courses during two separate drug challenges in nonhuman primates. (A) Time−activity curves of [^{18}F]GE-179 (bolus plus infusion) with a 0.6 mg/kg cold GE-179 drug challenge administered at the time indicated by the dotted gray line. Anatomical regions of interest in the brain and the arterial plasma curve are shown. (B) Corresponding representative CBV data and GLM fit for the putamen for the GE-179 drug challenge. (C) TACs of [^{18}F]GE-179 (bolus plus infusion) with a 0.6 mg/kg amphetamine drug challenge administered at the dotted gray line. Anatomical regions of interest in the brain and the arterial plasma curve are shown. (D) Corresponding representative CBV data and GLM fit for the putamen for the amphetamine challenge.

triggers cortical glutamate release.[24] We hypothesized that an acutely MA-activated brain would show a different population of open NMDA receptors than a vehicle-treated brain. We compared the TACs of the Ctx and Cb of rats that received MA or a mixture of MA and nonradioactive GE-179 2 min before radiotracer injection. Neither of these treatments changed the slope of the respective TACs compared with the whole-brain kinetics of the [^{18}F]GE-179 baseline signal.

Taken together, our preclinical imaging experiments with [^{18}F]GE-179 in rodents using direct competition, allosteric modulation, and orthogonal activation were not able to reveal an *in vivo* signal that directly correlates with NMDA receptor occupancy or activity.

NHP Imaging Using Simultaneous PET/MRI. PET/fMRI in NHPs was used to evaluate (i) [^{18}F]GE-179 PET signal modulation, (ii) hemodynamic changes due to pharmacological doses, and (iii) species differences as potential reasons for

DOI: 10.1021/acschemneuro.7b00327
ACS Chem. Neurosci. XXXX, XXX, XXX−XXX

Table 1. Percent Changes in [^{18}F]GE-179 Binding from Baseline Due to a Within-Scan Challenge of 0.6 mg/kg GE-179 or 0.6 mg/kg Amphetamine in Nonhuman Primates[a]

	putamen	caudate	thalamus	hippo- campus	prefrontal cortex	occipital lobe	cerebellum GM	GM	WM
GE-179	3.7	5.8	5.9	7.3	11.1	−4.3	−4.1	4.6	4.5
amphetamine	−11.7	−5.0	−3.1	−6.8	−3.8	−15.9	−16.6	−7.4	−7.3

[a]The baseline was calculated as the average signal for 15 min before the drug challenge, and the challenge was the average signal for the last 15 min of the data set.

nonspecific binding. The acquisition of dynamic PET and fMRI data enabled the evaluation of blood flow as a factor that has been suggested to influence the [^{18}F]GE-179 signal during pharmacological challenges.

Figure 3A shows representative voxelwise maps of the [^{18}F]GE-179 signal in NHP averaged over 20−50 min after a single-bolus injection. The corresponding TAC in Figure 3B shows that the kinetics in the NHP is largely identical with the human data, with the exception of minor differences in the uptake between brain regions.

To evaluate the effect of pharmacological challenges on the [^{18}F]GE-179 signal at steady state, a bolus-plus-infusion paradigm was employed for radiotracer administration. It was hypothesized that, given the reversible binding kinetics observed before, a pharmacological dose of cold GE-179 should reduce the brain signal by competitive displacement at the PCP binding site. Figure 4A shows TACs for anatomically defined regions from the blocking experiment with cold GE-179. The PET signal reached steady state about 35 min after tracer injection. At 46 min after injection, cold GE-179 (0.6 mg/kg) was administered, as indicated by the gray dotted line. Interestingly, the cold GE-179 challenge did not reduce the PET signal but rather led to an overall increase of 3.8 ± 4.0% on average over the measured anatomical regions, with the prefrontal cortex showing the largest signal increase (11.1%) and the putamen surprisingly showing the smallest signal increase (3.7%). A small decrease in [^{18}F]GE-179 binding was observed in two anatomical regions, the occipital lobe (−4.3%) and the cerebellum (−4.1%). The signal changes were sustained for the duration of the experiment, as displayed in Figure 4A. The differential effects in various anatomical regions did not correlate with known NMDA receptor distributions and showed relatively small overall signal changes due to the pharmacological dose of cold GE-179.

Arterial plasma blood levels of [^{18}F]GE-179 were not affected by administration of the cold compound, which demonstrates that delivery of the radiotracer did not change with the pharmacological dose of GE-179. Relative cerebral blood volume (CBV) as determined by fMRI was acutely reduced by cold GE-179 (Figure 4B). Interestingly, this is in contrast to previous reports on NMDA receptor blockers.[25] The measured decrease in CBV reflects a decrease in cerebral blood flow (CBF)[26] and because of the opposite sign should not be the cause of the observed [^{18}F]GE-179 signal increase.[27]

Combined, these data highlight that the *in vivo* [^{18}F]GE-179 PET brain signal cannot be "blocked" by unlabeled competition ligand and thus would not represent saturable or displaceable binding, as standardly defined by *in vivo* PET imaging. The reduction in CBV by GE-179 has no measurable effect on the PET signal, indicating that the signal is independent of flow, contrary to previous suggestions.[21] On the basis of this evaluation in rodents and NHPs with PET, the major part of the [^{18}F]GE-179 signal seems to be largely nonspecific. Our results thus indicate that [^{18}F]GE-179 is an inadequate tool for quantifying NMDA receptor availability.

Finally, we tested the application of [^{18}F]GE-179 as an activity-dependent brain imaging probe in NHPs. Even though open channel blockers at the PCP binding site typically display activity-dependent binding, previous evidence toward this functionality in [^{18}F]GE-179 imaging is partly contradicting: First, the anesthetized NHP brain should show different activity patterns than the awake human brain because of increased GABA-ergic activity. Second, the *in vivo* binding kinetics of [^{18}F]GE-179 in rodents, NHPs, and humans do not prove a trapped binding mechanism, which has been observed in cellular electrophysiology. In order to provide conclusive experimental evidence for activity-dependent [^{18}F]GE-179 binding *in vivo* in our study, we employed a bolus-plus-infusion paradigm including administration of a brain stimulant after the radiotracer infusion reached steady state. At 48 min after the injection of radiotracer (steady state), a bolus of amphetamine was administered (0.6 mg/kg i.v.). We hypothesized that according to the binding mechanism by open channel blocking, increased glutamatergic activity should lead to an increase in the regional [^{18}F]GE-179 signal. Figure 4C shows the resulting TACs from bolus-plus-infusion of [^{18}F]GE-179 for a range of anatomical regions in the NHP: the PET signal showed a small acute decrease that was sustained following amphetamine administration. The difference in the shapes of the TACs during uptake in Figure 4A vs Figure 4C can be attributed to small adjustments in the bolus/infusion ratios between the two experiments (see Methods for k_{bol} values). Table 1 lists the [^{18}F]GE-179 signal decreases due to amphetamine for different anatomical regions. The greatest [^{18}F]GE-179 signal decreases from baseline were observed in the cerebellum (−16.6%), occipital lobe (−15.9%), and putamen (−11.7%), and the smallest decreases were observed in the thalamus (−3.1%) and the prefrontal cortex (−3.8%). In line with previous observations,[28,29] the CBV signal due to amphetamine decreased acutely because of the dominant signaling from the inhibitory dopamine D2 receptor. This experiment could not provide evidence for the hypothesis of an activity-dependent [^{18}F]GE-179 signal *in vivo*.

Administration of psychostimulants like amphetamine and methamphetamine has been demonstrated to be associated with increased dopamine and glutamate release as well as NMDA synaptic currents.[30,31] An activity-dependent NMDA probe would thus be expected to exhibit a signal increase in mesocorticolimbic areas with amphetamine administration. However, we observed a widespread decrease in signal. Even though there is some evidence that amphetamine can inhibit the NMDA receptor directly or decrease NMDA signaling,[32,33] the amphetamine dose administered in our experiment would be expected to elicit a much stronger and anatomically specific change in signal. Both amphetamine and cold GE-179 elicited only an overall small signal change even though the administered doses were large and are known to affect

DOI: 10.1021/acschemneuro.7b00327
ACS Chem. Neurosci. XXXX, XXX, XXX−XXX

NMDA receptors, suggesting that the probe is limited in its detection capability for NMDA activity.

Molecular imaging of NMDA receptors remains a challenge. Our extensive preclinical experiments using the NMDA pore blocker [^{18}F]GE-179 were not able to demonstrate displaceable *in vivo* binding or predictable signal manipulation that provides evidence for an *in vivo* activity-dependent NMDA signal in rats and NHPs. We thus recommend interpreting existing and future studies using [^{18}F]GE-179 in light of signal changes of the radiotracer probe rather than NMDA activity.

METHODS

Radiotracer Synthesis. [^{18}F]GE-179 was synthesized using a thiophenol precursor purchased from GE Healthcare (Amersham, UK) for [^{18}F]fluoroethylation as previously described.[15] Briefly, the radionuclide ^{18}F and the common alkylation building block [^{18}F]-fluoroethyl tosylate (FETs) were synthesized as described earlier in our lab.[34] Freshly prepared FETs was added to 0.8 mg of precursor and 0.5 mg of K_2CO_3 as a solution in 0.5 mL of acetonitrile. This mixture was heated to 100 °C until all of the FETs was fully reacted, as determined by radio-HPLC (typically 10−15 min). The crude mixture was diluted in 10 mL of sterile water and passed through a strataX reversed-phase solid-phase extraction cartridge. In order to remove unreacted precursor, the cartridge was washed with 10 mL of 9:1 (v/v) 0.1 M ammonium formate/acetonitrile followed by 10 mL of sterile water. Clean [^{18}F]GE-179 was eluted with absolute ethanol (1 mL) diluted with saline (9 mL) and passed through a sterile membrane filter (0.22 μm) into a sterile evacuated vial ready for injection for imaging experiments in rodents and NHPs. The purity and identity of the radiolabeled compound were confirmed using UV (list wavelength) and radio-HPLC (reference standard provided purchased by GE and confirmed by LC−MS).

Preparation of Pharmacological Challenges. The drugs MK801, PCP, ifenprodil, MA, and amphetamine, which were used for the pharmacological challenges in the rats and NHPs, were obtained from Sigma-Aldrich (St. Louis, MO, USA). Unlabeled GE-179 was purchased from GE Healthcare. MK801 and PCP were formulated in saline + 10% EtOH, ifenprodil and GE-179 in saline + 10% 1:1 (v/v) DMSO/Tween 80, MA and amphetamine in saline on the day of the experiment. Ketamine was obtained in liquid formulation and diluted in saline to the appropriate concentration. All of the treatment and imaging experiments were performed according to procedures approved by the Institutional Animal Care and Use Committee of Massachusetts General Hospital.

Rat Experimental Design, Image Acquisition, and Analysis. Sprague−Dawley rats (n = 12, 250−500 g) were anesthetized using isoflurane inhalation (1−2% with oxygen carrier), and the depth of anesthesia was controlled by maintaining a breathing rate of ∼60 min^{-1}. Animals were placed in a Triumph PET/CT scanner, and dynamic scanning was initiated 10 s prior to injection of [^{18}F]GE-179. At the end of the PET scan, a CT scan was performed for attenuation correction and anatomical reference. Imaging data were reconstructed in increasing time frames using the MLEM method and analyzed using PMOD and AMIDE software.

NHP Experimental Design. Two animals (male *Rhesus macaques*) underwent PET/MRI. For each study, the animal was anesthetized, initially with 10 mg/kg ketamine and 0.5 mg/kg xylazene, and maintained with isoflurane (∼1%, mixed with oxygen) after intubation. A timespan of ∼2 h was ensured between the initial ketamine administration and injection of the radiotracer to allow for the washout of ketamine and to minimize any direct blocking effects due to ketamine. All of the studies and procedures complied with the regulations of the Institutional Animal Care and Use Committee of Massachusetts General Hospital. For the baseline study, a bolus of 4.5 mCi of [^{18}F]GE-179 was injected intravenously. On the basis of the single-bolus injection kinetics, bolus-plus-infusion parameters were calculated.[35] On the basis of this protocol, equilibrium should be reached within 30−40 min, and thus, the time points for the drug challenges were chosen to occur beyond that time for predictable signal manipulation. For the cold GE-179 challenge experiment, a bolus of 3.0 mCi was followed by continuous infusion of 3.6 mCi over the course of 100 min (k_{bol} = 84 min). For the amphetamine challenge, a bolus of 3.0 mCi was followed by continuous infusion of 4.0 mCi (k_{bol} = 75 min). For monitoring of the overall [^{18}F]GE-179 blood concentration, arterial blood (venous blood for the baseline study) was taken throughout the experiment. By means of simultaneous fMRI, cerebral blood volume was calculated in order to correlate CBV changes to the PET signal.

NHP Image Acquisition. Simultaneous PET and MRI data were acquired on a prototype scanner consisting of a BrainPET insert and a Tim Trio 3T MRI scanner (Siemens AG, Healthcare Sector, Erlangen, Germany). A custom-built PET-compatible eight-channel NHP receiver array together with a vendor-supplied local circularly polarized transmitter coil was used for MRI.[36] An anatomical T_1-weighted MRI (MEMPRAGE)[37] was acquired at the beginning of the scan session. To improve the fMRI detection power, ferumoxytol (Feraheme, AMAG Pharmaceuticals, Cambridge, MA) was injected at 10 mg/kg prior to fMRI and radiotracer injection. Whole-brain fMRI data were then acquired throughout the remainder of the scanning session with multislice echo-planar imaging (EPI) at 2-fold acceleration that had an isotropic resolution of 1.3 mm and a temporal resolution of 3 s. Other parameters included FOV_{MR} = 110 × 72.8 mm^2, BW = 1350 Hz/pixel, flip angle = 60°, and an echo time (TE) of 23 ms.

PET emission data were acquired in list-mode format for 100 min starting with radiotracer injection. Images were reconstructed with a standard 3D Poisson ordered-subset expectation maximization algorithm using prompt and variance-reduced random coincidence events. Normalization, scatter, and attenuation sinograms (including attenuation of the radiofrequency coil) were included in the reconstruction. The reconstructed volume consisted of 1.25 mm × 1.25 mm × 1.25 mm voxels in a 256 × 256 × 153 matrix, which were downsampled by a factor of 2 postreconstruction. The framing intervals were 10 × 1 min and 5 × 2 min followed by 5 min frames.

NHP Functional Image Analysis. PET and MRI data were registered to the Saleem−Logothetis stereotaxic space[38] with an affine transformation (12 degrees of freedom) using a multisubject MRI template[39] in which anatomical regions of interest were defined. After motion correction (AFNI software) and spatial smoothing of fMRI data with a 2.5 mm Gaussian kernel, statistical analysis was carried out using the general linear model (GLM). The temporal response to the drug injection was modeled with a gamma-variate function, in which the time to peak was adjusted to minimize the χ^2/DOF of the GLM fit to the data. The resulting signal changes were converted to percent changes in CBV by previously described methods.[40] All PET and fMRI data analysis and generation of parametric images from voxelwise kinetic modeling were generated with open-access software (www.nitrc.org/projects/jip).

AUTHOR INFORMATION

Corresponding Author

*Address: Athinoula A. Martinets Center for Biomedical Imaging, Department of Radiology, Massachusetts General Hospital, 149 13th Street, Suite 2301, Charlestown, MA 02129. Phone: (617) 726-9034. E-mail: csander@mgh.harvard.edu.

ORCID

Frederick A. Schroeder: 0000-0003-0469-4196

Jacob M. Hooker: 0000-0002-9394-7708

Christin Y. Sander: 0000-0001-6003-8615

Author Contributions

C.Y.S. and M.S. designed and conducted the experiments, performed data analysis, interpreted the results, and wrote the manuscript. F.A.S. and M.S.P. helped to conduct the experiments and edited the manuscript. R.L.C., B.R.R., and J.M.H. provided insight into interpretation of the results and edited the manuscript.

DOI: 10.1021/acschemneuro.7b00327
ACS Chem. Neurosci. XXXX, XXX, XXX−XXX

Funding

This research was supported through a collaborative research agreement from GE Global Research (Niskayuna, NY, USA). Further support included grants from the National Institutes of Health (NIH) (P41EB015896, S10RR026666, S10RR022976, S10RR019933, and S10RR017208). M.S. was supported by the MSCA fellowship INSCAPE from the REA of the European Commission. J.M.H. received support from the Phyllis and Jerome Lyle Rappaport MGH Research Scholar Award. C.Y.S. received support from NIH grant K99DA043629.

Notes

The authors declare the following competing financial interest(s): This research was supported by a collaborative research agreement from GE Global Research.

■ ACKNOWLEDGMENTS

We thank Helen Deng, Grae Arabasz, Regan Butterfield, and Shirley Hsu for their help with scanning and NHP experiments.

■ REFERENCES

(1) Paoletti, P., Bellone, C., and Zhou, Q. (2013) NMDA receptor subunit diversity: impact on receptor properties, synaptic plasticity and disease. *Nat. Rev. Neurosci. 14*, 383−400.

(2) Iacobucci, G. J., and Popescu, G. K. (2017) NMDA receptors: linking physiological output to biophysical operation. *Nat. Rev. Neurosci. 18*, 236−249.

(3) Traynelis, S. F., Wollmuth, L. P., McBain, C. J., Menniti, F. S., Vance, K. M., Ogden, K. K., Hansen, K. B., Yuan, H., Myers, S. J., and Dingledine, R. (2010) Glutamate receptor ion channels: structure, regulation, and function. *Pharmacol. Rev. 62*, 405−96.

(4) Hunt, D. L., and Castillo, P. E. (2012) Synaptic plasticity of NMDA receptors: mechanisms and functional implications. *Curr. Opin. Neurobiol. 22*, 496−508.

(5) Karakas, E., and Furukawa, H. (2014) Crystal structure of a heterotetrameric NMDA receptor ion channel. *Science (Washington, DC, U. S.) 344*, 992−997.

(6) Karakas, E., and Furukawa, H. (2014) Crystal structure of a heterotetrameric NMDA receptor ion channel. *Science 344*, 992−997.

(7) Monaghan, D. T., and Jane, D. E. (2009) Pharmacology of NMDA Receptors, in *Biology of the NMDA Receptor* (VanDongen, A. M., Ed.), Chapter 12, CRC Press, Boca Raton, FL.

(8) Fuchigami, T., Nakayama, M., and Yoshida, S. (2015) Development of PET and SPECT probes for glutamate receptors. *Sci. World J. 2015*, 716514.

(9) Volgraf, M., Sellers, B. D., Jiang, Y., Wu, G., Ly, C. Q., Villemure, E., Pastor, R. M., Yuen, P., Lu, A., Luo, X., Liu, M., Zhang, S., Sun, L., Fu, Y., Lupardus, P. J., Wallweber, H. J. A., Liederer, B. M., Deshmukh, G., Plise, E., Tay, S., Reynen, P., Herrington, J., Gustafson, A., Liu, Y., Dirksen, A., Dietz, M. G. A., Liu, Y., Wang, T.-M., Hanson, J. E., Hackos, D., Scearce-Levie, K., and Schwarz, J. B. (2016) Discovery of GluN2A-Selective NMDA Receptor Positive Allosteric Modulators (PAMs): Tuning Deactivation Kinetics via Structure-Based Design. *J. Med. Chem. 59*, 2760−2779.

(10) Maolanon, A. R., Risgaard, R., Wang, S.-Y., Snoep, Y., Papangelis, A., Yi, F., Holley, D., Barslund, A. F., Svenstrup, N., Hansen, K. B., and Clausen, R. P. (2017) Subtype-Specific Agonists for NMDA Receptor Glycine Binding Sites. *ACS Chem. Neurosci. 8*, 1681−1687.

(11) MacDonald, J. F., Bartlett, M. C., Mody, I., Pahapill, P., Reynolds, J. N., Salter, M. W., Schneiderman, J. H., and Pennefather, P. S. (1991) Actions of ketamine, phencyclidine and MK-801 on NMDA receptor currents in cultured mouse hippocampal neurones. *J. Physiol. 432*, 483−508.

(12) Bolshakov, K. V., Gmiro, V. E., Tikhonov, D. B., and Magazanik, L. G. (2003) Determinants of trapping block of N-methyl-d-aspartate receptor channels. *J. Neurochem. 87*, 56−65.

(13) Blanpied, T. A., Boeckman, F. A., Aizenman, E., and Johnson, J. W. (1997) Trapping channel block of NMDA-activated responses by amantadine and memantine. *J. Neurophysiol. 77*, 309−23.

(14) Dumont, F., Sultana, A., and Waterhouse, R. N. (2002) *Bioorg. Med. Chem. Lett. 12*, 1583−1586.

(15) Robins, E. G., Zhao, Y., Khan, I., Wilson, A., Luthra, S. K., and Årstad, E. (2010) Synthesis and in vitro evaluation of 18F-labelled S-fluoroalkyl diarylguanidines: Novel high-affinity NMDA receptor antagonists for imaging with PET. *Bioorg. Med. Chem. Lett. 20*, 1749−1751.

(16) Walters, M. R., Bradford, A. P. J., Fischer, J., and Lees, K. R. (2002) Early clinical experience with the novel NMDA receptor antagonist CNS 5161. *Br. J. Clin. Pharmacol. 53*, 305−311.

(17) Waterhouse, R. N., Slifstein, M., Dumont, F., Zhao, J., Chang, R. C., Sudo, Y., Sultana, A., Balter, A., and Laruelle, M. (2004) In vivo evaluation of [11C]N-(2-chloro-5-thiomethylphenyl)- N′-(3-methoxy-phenyl)-N′-methylguanidine ([11C]GMOM) as a potential PET radiotracer for the PCP/NMDA receptor. *Nucl. Med. Biol. 31*, 939−948.

(18) Martin, D. C., Plagenhoef, M., Abraham, J., Dennison, R. L., and Aronstam, R. S. (1995) Volatile anesthetics and glutamate activation of N-methyl-D-aspartate receptors. *Biochem. Pharmacol. 49*, 809−817.

(19) Knol, R. J. J., De Bruin, K., Van Eck-Smit, B. L. F., Pimlott, S., Wyper, D. J., and Booij, J. (2009) In vivo [123I]CNS-1261 binding to D-serine-activated and MK801-blocked NMDA receptors: A storage phosphor imaging study in rats. *Synapse 63*, 557−564.

(20) Waterhouse, R. N. (2003) Imaging the PCP site of the NMDA ion channel. *Nucl. Med. Biol. 30*, 869−878.

(21) McGinnity, C. J., Hammers, A., Barros, D. A. R., Luthra, S. K., Jones, P. A., Trigg, W., Micallef, C., Symms, M. R., Brooks, D. J., Koepp, M. J., and Duncan, J. S. (2014) Initial Evaluation of 18F-GE-179, a Putative PET Tracer for Activated *N*-Methyl-D-Aspartate Receptors. *J. Nucl. Med. 55*, 423−430.

(22) McGinnity, C. J., Koepp, M. J., Hammers, A., Riaño Barros, D. A., Pressler, R. M., Luthra, S., Jones, P. A., Trigg, W., Micallef, C., Symms, M. R., Brooks, D. J., and Duncan, J. S. (2015) NMDA receptor binding in focal epilepsies. *J. Neurol., Neurosurg. Psychiatry 86*, 1150−1157.

(23) Tyler, M. W., Yourish, H. B., Ionescu, D. F., and Haggarty, S. J. (2017) Classics in Chemical Neuroscience: Ketamine. *ACS Chem. Neurosci. 8*, 1122−1134.

(24) Parsegian, A., and See, R. E. (2014) Dysregulation of Dopamine and Glutamate Release in the Prefrontal Cortex and Nucleus Accumbens Following Methamphetamine Self-Administration and During Reinstatement in Rats. *Neuropsychopharmacology 39*, 811−822.

(25) Gozzi, A., Large, C. H., Schwarz, A., Bertani, S., Crestan, V., and Bifone, A. (2008) Differential Effects of Antipsychotic and Glutamatergic Agents on the phMRI Response to Phencyclidine. *Neuropsychopharmacology 33*, 1690−1703.

(26) Grubb, R. L., Raichle, M. E., Eichling, J. O., and Ter-Pogossian, M. M. (1974) The Effects of Changes in PaCO2 Cerebral Blood Volume, Blood Flow, and Vascular Mean Transit Time. *Stroke 5*, 630−639.

(27) Sander, C. Y., Mandeville, J. B., Wey, H.-Y., Catana, C., Hooker, J. M., and Rosen, B. R. (2017) Effects of flow changes on radiotracer binding: Simultaneous measurement of neuroreceptor binding and cerebral blood flow modulation. *J. Cereb. Blood Flow Metab.*, 0271678X17725418.

(28) Choi, J.-K., Chen, Y. I., Hamel, E., and Jenkins, B. G. (2006) Brain hemodynamic changes mediated by dopamine receptors: Role of the cerebral microvasculature in dopamine-mediated neurovascular coupling. *NeuroImage 30*, 700−712.

(29) Mandeville, J. B., Sander, C. Y. M., Jenkins, B. G., Hooker, J. M., Catana, C., Vanduffel, W., Alpert, N. M., Rosen, B. R., and Normandin, M. D. (2013) A receptor-based model for dopamine-induced fMRI signal. *NeuroImage 75*, 46−57.

(30) Lominac, K. D., Sacramento, A. D., Szumlinski, K. K., and Kippin, T. E. (2012) Distinct neurochemical adaptations within the nucleus accumbens produced by a history of self-administered vs non-

DOI: 10.1021/acschemneuro.7b00327
ACS Chem. Neurosci. XXXX, XXX, XXX−XXX

contingently administered intravenous methamphetamine. *Neuropsychopharmacology 37*, 707−22.
(31) Li, M., Underhill, S. M., Reed, C., Phillips, T. J., Amara, S. G., and Ingram, S. L. (2017) Amphetamine and Methamphetamine Increase NMDAR-GluN2B Synaptic Currents in Midbrain Dopamine Neurons. *Neuropsychopharmacology 42*, 1539−1547.
(32) Yeh, G.-C., Chen, J.-C., Tsai, H.-C., Wu, H.-H., Lin, C.-Y., Hsu, P.-C., and Peng, Y.-C. (2002) Amphetamine Inhibits the *N*-Methyl-D-Aspartate Receptor- Mediated Responses by Directly Interacting with the Receptor/Channel Complex. *J. Pharmacol. Exp. Ther. 300*, 1008−1016.
(33) Lee, K. W., Kim, H. C., Lee, S. Y., and Jang, C. G. (2011) Methamphetamine-sensitized mice are accompanied by memory impairment and reduction of N-methyl-d-aspartate receptor ligand binding in the prefrontal cortex and hippocampus. *Neuroscience 178*, 101−107.
(34) Hooker, J. M., Strebl, M. G., Schroeder, F. A., Wey, H.-Y., Ambardekar, A. V., McKinsey, T. A., and Schoenberger, M. (2017) Imaging cardiac SCN5A using the novel F-18 radiotracer radiocaine. *Sci. Rep. 7*, 42136.
(35) Endres, C. J., Kolachana, B. S., Saunders, R. C., Su, T., Weinberger, D., Breier, A., Eckelman, W. C., and Carson, R. E. (1997) Kinetic Modeling of [11C]Raclopride: Combined PET-Microdialysis Studies. *J. Cereb. Blood Flow Metab. 17*, 932−942.
(36) Sander, C. Y., Keil, B., Chonde, D. B., Rosen, B. R., Catana, C., and Wald, L. L. (2015) A 31-channel MR brain array coil compatible with positron emission tomography. *Magn. Reson. Med. 73*, 2363−2375.
(37) van der Kouwe, A. J. W., Benner, T., Salat, D. H., and Fischl, B. (2008) Brain morphometry with multiecho MPRAGE. *NeuroImage 40*, 559−569.
(38) Saleem, K. S., and Logothetis, N. (2012) *A Combined MRI and Histology Atlas of the Rhesus Monkey Brain in Stereotaxic Coordinates*, 2nd ed., Academic Press, London.
(39) McLaren, D. G., Kosmatka, K. J., Oakes, T. R., Kroenke, C. D., Kohama, S. G., Matochik, J. A., Ingram, D. K., and Johnson, S. C. (2009) A population-average MRI-based atlas collection of the rhesus macaque. *NeuroImage 45*, 52−59.
(40) Mandeville, J. B., Marota, J. J. A., Kosofsky, B. E., Keltner, J. R., Weissleder, R., Rosen, B. R., and Weisskoff, R. M. (1998) Dynamic functional imaging of relative cerebral blood volume during rat forepaw stimulation. *Magn. Reson. Med. 39*, 615−624.

DOI: 10.1021/acschemneuro.7b00327
ACS Chem. Neurosci. XXXX, XXX, XXX−XXX